ACS OMEGA

Open Access

http://pubs.acs.org/journal/acsodf

Article

Dissipative Particle Dynamics-Based Simulation of the Effect of Asphaltene Structure on Oil−Water Interface Properties

Chonghao Liang, Xiaoyan Liu,* Hui Jiang, Ying Xu, and Yongying Jia

Cite This: *ACS Omega* 2023, 8, 33083−33097

Read Online

ACCESS | Metrics & More | Article Recommendations

ABSTRACT: Asphaltenes are the main substances that stabilize emulsions during the production, processing, and transport of crude oil. The purpose of this research is to investigate the process of asphaltenes forming interfacial films at the oil−water interface by means of dissipative particle dynamics (DPD) and the effect of asphaltenes of different structures on the oil−water interface during the formation of interfacial film. It is demonstrated that the thickness of the interfacial film formed at the oil−water interface gradually increases as the asphaltene concentration rises and the amount of asphaltene adsorbed at the oil−water interface gradually multiplies. Both the number and type of heteroatoms in asphaltenes affect the interfacial behavior of asphaltenes. The interface activity of asphaltenes can be enhanced by increasing the number of heteroatoms in the asphaltene, and the type of heteroatom affects as well the interfacial activity of the asphaltene as it affects the aggregation behavior of the asphaltene in the system. As the number of asphaltene aromatic rings increases, the oil−water interfacial tension (IFT) trends down gradually, while the effect of alkyl side chains on the reduction of IFT of asphaltenes is different, and asphaltenes with medium length alkyl side chains can reduce IFT more efficiently.

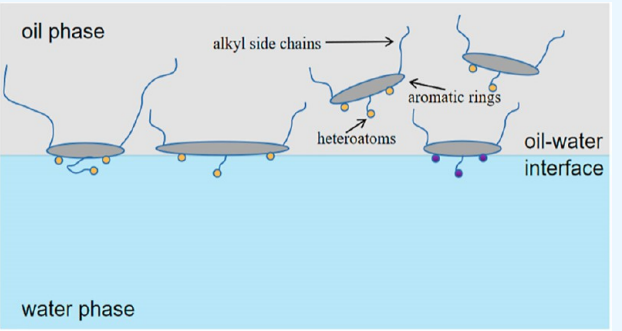

1. INTRODUCTION

The investigation of the stability of emulsions is of significant importance for processes, such as oil production, processing, and transportation.[1−8] Asphaltenes in crude oil components play an essential role in stabilizing emulsions because asphaltenes are a naturally occurring surface active substance.[9] It is indicated that the asphaltene molecular composition consists of three main components, which are heteroatoms with hydrophilic properties, a polycyclic aromatic core, and aliphatic alkyl side chains.[10−14] The specific structure of asphaltene molecules provides them a certain surface activity, so asphaltenes may be a crucial factor in the stabilization of the oil−water interface of emulsions.[15−17] It has been revealed that the main factor that makes the emulsion oil−water interface stable is the formation of an interfacial film or elastic layer at the oil−water interface of asphaltenes with natural surface activity.[1,7,8]

In recent years, research on the effect of asphaltene on the stability of the oil−water interface have received increasing attention.[16,18−21] Orbulescu et al.[22] studied the morphology of asphaltene films at the oil−water interface by atomic force microscopy (AFM) and investigated the process of breaking the asphaltene film layer by emulsion breakers. Feng et al.[23] examined the state of asphaltene film formation and destruction by using micropipettes. Larichev et al.[24] studied the effect of different organic solvents on the size and shape of asphaltene agglomerates using small-angle X-ray scattering and scanning tunneling microscopy. Wang et al.[25] investigated the mechanism associated with the reduction of oil−water interfacial tension by asphaltenes using dynamic interfacial tension equations. The results indicate that the concentration of asphaltene has an effect on its adsorption and coverage at the interface. You et al.[26] investigated the effect of the asphaltene aggregation state on the structure-related properties of the model oil/brine interface using the pendant drop method and further investigated the relationship between the structural properties of the interface and the macroscopic stability of the emulsion. Cagna et al.[27] investigated the reversibility of asphaltene adsorption at the oil−water interface and the results of the study confirmed that asphaltene adsorption at the oil−water interface is irreversible. Yang et al.[4] investigated asphaltene subcomponents stabilizing the oil−water interface layer. The results demonstrate that the IAA subcomponent is the main factor in emulsion stability and the

Received: July 27, 2023
Accepted: August 14, 2023
Published: August 30, 2023

formation of a rigid water−oil interface. Liu et al.[17] applied droplet morphology analysis to investigate the effect of synergistic interaction between gum and asphaltenes on the properties of the water−oil interface and the stability of emulsions. The research confirmed the synergistic interaction between asphaltenes and gums. The addition of gum enhanced the interfacial affinity of asphaltenes at the initial stage of adsorption. The long-term adsorption capacity of asphaltenes was stronger than that of gums. Ma et al.[28] examined the stability and instability mechanisms of the interfacially active asphaltene-stabilized water-in-oil emulsions. It was shown that the reconstruction of hydrogen bonds promoted the rupture of IAA films at the oil−water interface, allowing water droplets to cluster and merge in the oil phase. These research studies have contributed significantly to the academic recognition of the mechanism of asphalt-stabilized emulsions. However, experimental studies on the effect of asphaltenes on emulsion cannot explain the mechanism of asphaltene interfacial film formation and emulsion stabilization from a molecular perspective. In contrast, computer simulation techniques, such as molecular mechanics (MM), molecular dynamics simulation (MD), Monte Carlo simulation (MC), Brownian dynamics simulation (BD), and dissipative particle dynamics simulation (DPD) can effectively compensate for the experimental deficiencies.

Mikami et al.[29] demonstrated the interaction of asphaltenes at the oil−water interface through MD simulations. The research demonstrated that the aggregation of asphaltene molecules at the oil−water interface can greatly reduce the oil−water interfacial tension,[25,30] and when the oil−water interface is rich in asphaltenes, a complete interfacial film can be formed at the oil−water interface. Ruiz-Morales and Mullins[31] investigated the orientation of asphaltenes at the oil−water interface through DPD simulation, using toluene as the oil model. The simulation shows that the asphaltene model forms three contact angles with the oil−water interface, horizontal, vertical, and 45° inclined. The asphaltene aromatic nucleation zone is located at the oil−water interface, and the alkyl side chains are located in the oil zone. When the asphaltene concentration is relatively high, some asphaltenes migrate to the oil phase due to blockage and spatial repulsion, while some asphaltenes continue to adsorb at the oil−water interface. Chen et al.[32] examined the aggregation and orientation behavior of asphaltene molecules at the interface of crude oil water-bearing emulsion using dissipative particle dynamics methods. The results showed that initially disordered asphaltenes assemble into nanoclusters of multiple molecules, with most of the orphan asphaltene polycyclic aromatic layers tending to be perpendicular to the oil−water interface, while most of the archipelagic asphaltene polycyclic aromatic layers tend to be parallel to the oil−water interface. Both nanoaggregate structures formed a stable interfacial film at the oil−water interface, which hindered the aggregation between water droplets. de Oliveira et al.[33] researched the interfacial properties of asphaltene molecules at the oil−water interface by means of dissipative particle dynamics. When the asphaltene concentration is relatively low, the asphaltene molecules are preferentially parallel to the interface; while at high asphaltene concentrations, the molecules exhibit a tilted structure. Moreover, at low asphaltene concentrations, the asphaltene molecules form small aggregates, while at greater asphaltene concentrations, they form larger structures. Jian et al.[30] examined the effect of asphaltene concentration on the oil−water interfacial tension (IFT) using the droplet technique and molecular dynamics (MD) simulations. The results indicate for the first time the coupling effect of temperature and asphaltene concentration on interfacial tension.

Asphaltene structure (heteroatoms, number of aromatic rings, and alkyl side chains) has a significant effect on their aggregation behavior in the system.[10,11,34−40] Jian et al.[36] explored the effect of alkyl side-chain length on asphaltene aggregation in water by molecular dynamics simulations (MD). The simulation results showed that there was a non-monotonic relationship between the degree of asphaltene aggregation in water and alkyl side chains. Asphaltenes with either an extremely long or an exceedingly short alkyl side chain are able to form dense aggregates, while asphaltenes of medium length are incapable of forming larger aggregates. Rahmati[34] investigated the properties of asphaltene heteroatoms and alkyl side chains on their aggregation in aromatic solvents using a molecular dynamics (MD) approach. The results indicate that asphaltene aggregation intensely depends on the type and number of heteroatoms in the asphaltene structure, while the length and number of alkyl side chains in the asphaltene structure also have an essential effect on the degree of aggregation. Sedghi et al.[37] suggested that the interaction between stacked polycyclic aromatic hydrocarbons (PAHs) on top of each other is the driving force for asphaltene aggregation. The strength of such an interaction depends not only on the number of aromatic rings but also on the presence of heteroatoms in the aromatic nuclei that reduce electrostatic repulsion. Scholars have mainly focused on the effect of the asphaltene structure on its aggregation behavior in solvents,[11,34−37,41,42] while studies on the effect of asphaltene structure on the oil−water interface have not been reported. Therefore, it is significant to explore the effect of asphaltene structure on the oil−water interface and investigate the mechanism of different structures on asphaltene film formation at the oil−water interface.

Dissipative particle dynamics can simulate the relevant behavior of molecules at the oil−water interface at large time and space scales,[43−47] which can effectively reveal the molecular dynamic evolution of asphaltenes at the oil−water interface. Although a large number of studies have been carried out on asphaltene films at the oil−water interface, the effect of different structures of asphaltenes (including heteroatoms, aromatic rings, and alkyl side chains) on the oil−water interface is still worthy of further study. This investigation builds on previous research by Ruiz-Morales and Mullins[31,48] using dissipative particle dynamics (DPD) methods to research the behavior of different asphaltene structures at the oil−water interface. The mechanism of asphaltene stabilization at the oil−water interface is revealed by exploring the process of asphaltene film formation at the interface and the effect of its structure on film formation. As a result of this research, we are enabled to obtain a deeper understanding of the role of asphaltenes in the production, processing, and transport of crude oil.

2. RESEARCH METHODS AND MODELS

2.1. DPD Method. Dissipative particle dynamics, which was first proposed by Hoogerbrugge and Koelman,[49] is a coarse-grained simulation technique for modeling complex fluid systems at long times and large scales. Each bead in the coarse-grained models embodies a group of atoms. In DPD simulations, the beads are connected using a spring model where each bead represents a set of molecules or atoms and all

https://doi.org/10.1021/acsomega.3c05486
ACS Omega 2023, 8, 33083−33097

the beads in the system interact through three forces.[43,44] These three forces are the conservative force, the dissipative force, and the random force, which act between two particles i and j at a distance of r_{ij}.[50−53]

$$F_i = \sum_{i \neq j} (F_{ij}^{C} + F_{ij}^{D} + F_{ij}^{R}) \tag{1}$$

where F_i is the force exerted on this bead, and this force is the sum of the conservative, random, and dissipative forces. F_{ij}^{C} in the formula is the conservative force, F_{ij}^{D} is the dissipative force, and F_{ij}^{R} is the random force. Where F_{ij}^{C} is the conservative force between the ith bead and the jth bead, and the conservative force is usually written as[54]

$$F_{ij}^{C} = \begin{cases} a_{ij}(1 - r_{ij}/r_c)r_{ij} & (r_{ij} < r_c) \\ 0 & (r_{ij} \geq r_c) \end{cases} \tag{2}$$

where r_{ij} is the distance between the ith bead and the jth bead. $\hat{r}_{ij}$ is the unit vector that represents the direction from bead i to bead j. r_c is the cutoff radius, which indicates the range of interaction between the beads. The other two forces in eq 3 are the random force F_{ij}^{R} and the dissipative force F_{ij}^{D}. It is expressed as follows[54,55]

$$F_{ij}^{R} = \sigma w^{R}(r_{ij})\theta_{ij}\hat{r}_{ij} \tag{3}$$

$$F_{ij}^{D} = -\eta w^{D}(r_{ij})(\hat{r}_{ij} \times v_{ij})\hat{r}_{ij} \tag{4}$$

$$\omega^{R}(r_{ij}) = \sqrt{\omega^{D}(r_{ij})} = \begin{cases} 1 - r_{ij} & (r_{ij} < r_c) \\ 0 & (r_{ij} \geq r_c) \end{cases} \tag{5}$$

$$\sigma^2 = 2\eta k_B T \tag{6}$$

σ in the formula is the noise amplitude and ω^{D} and ω^{R} represent the weight functions of dissipative force and random force, respectively. As shown in eq 5, to sample the distribution of the regular system synthesis, the fluctuation−dissipation theorem must be obeyed. r_{ij} is the distance between two beads, θ_{ij} denotes a random number with zero mean and zero unit variance, and η is the dissipative force amplitude.[56] As shown in eq 6 above, the combined action of the random force and dissipative force is equivalent to a thermostat that maintains momentum and can guarantee correct hydrodynamics on a sufficiently long time and space scale.[44,57]

The conservative force is a soft repulsive force that can be calculated by the Flory−Huggins binary interaction parameter.[48,58]

$$a_{ij} = a_{ii} + 3.5\chi_{ij} \tag{7}$$

$$\chi_{ij} = \frac{v_{ij}}{RT}(\delta_i - \delta_j)^2 \tag{8}$$

In eq 7, a_{ij} is the parameter of repulsive force between different types of beads and a_{ii} is the parameter of repulsive force between the same type of beads. In this study, we used $a_{ii} = 25$ and it was shown that the simulation gives more accurate values of oil−water interfacial tension when $a_{ii} = 25$.[45,59] In eq 8, v_{ij} is the average molar volume of the substance, R is the gas constant, T is the absolute temperature, and δ_i and δ_j are the solubility parameters of system i and system j.

2.2. Coarse Graining Model. The box size was selected to be 100 Å × 100 Å × 200 Å, and the system consisted of two regions: one part was the aqueous phase region and the other part was the oil phase region. Toluene has been used as an oil model and the reason for its feasibility is that the solubility parameters of toluene are similar to those of oil.[16,31,45,48] At the same time, a given concentration of asphaltene is put into the oil phase zone. The total number of beads in the DPD system can be obtained from eq 9.[48]

$$N_b = \frac{\rho V_{Box}}{r_c^3} \tag{9}$$

In eq 11, N is the total number of beads in the system, V_{Box} denotes the total volume of the simulated system box, ρ is the density of the beads in the simulated system, and r_c is the radius of the beads.

The concentration of asphaltene in the simulated system can be calculated from the following eqs 10 and 11.[48]

$$C_R = \frac{n_{\text{coarse-grained molecules}}}{V_{\text{R-Box}}} = \frac{C^{\text{physical}}}{b} \tag{10}$$

$$V_{\text{R-Box}} = \frac{V_{\text{Box}}^{\text{physical}}}{r_c^3} \tag{11}$$

Where C_R is the reduced concentration, $n_{\text{coarse-grained molecule}}$ is the amount of coarse-grained asphaltene in the system, and $V_{\text{R-Box}}$ is the reduced volume of the simulated box. C_{physical} is physical molar concentrations. b are DPD concentration units, which is equal to 6.1 mol/L for $N_m = 3$. $V_{\text{Box}}^{\text{physical}}$ is the physical volume in the simulation and r_c is the cutoff radius.

The interfacial tension at the toluene−water interface is determined at the end of the simulation and the interfacial tension is calculated from eq 12 as follows.[48,60,61]

$$\text{IFT} = \frac{1}{2}\left(P_{zz} - \frac{P_{xx} + P_{yy}}{2}\right)L_z \tag{12}$$

Where P_{xx}, P_{yy}, and P_{zz} are the diagonal components of the stress tensor of the equilibrium system. L_z is the length of the z-frame edge. A factor of $K_B T/r_c^2$ is used in the simulation system to convert DPD units to real units. The factor 1/2 in eq 14 is due to the fact that the simulated system forms two interfaces.

The coarse-grained model configurations of asphaltene, water, and oil molecules in the simulation are shown in Figure 1.

The molecular structure of asphaltenes has been shown in many studies to be composed of aromatic rings, alkyl side chains, and heteroatoms.[13,14,40] The asphaltene structure used in this paper is based on the Yen-mullins model of asphaltenes presented by Ruiz-Morales et al.[13,14,31,48] Based on the Yen-mullins model of asphaltenes, the asphaltene model was modified by altering the type and number of heteroatoms in the basic structure of the asphaltene molecule, the number of central polycyclic aromatic rings, and the length of the alkyl side chains.[34,35] The basic asphaltene structure consists of three types of beads,[12,31] namely, B-bead, H-bead, and M/T-beads. The B bead represents the aromatic ring portion, the H bead represents the alkyl side-chain portion, the M bead represents the oxygen-containing elemental heteroatom in the asphaltene, and the T bead represents the non-oxygen-containing elemental heteroatom in the asphaltene.[32,55,62] The asphaltene molecules constructed in the simulations are shown in Figures 2, 3, 4 and 5.

https://doi.org/10.1021/acsomega.3c05486
ACS Omega 2023, 8, 33083−33097

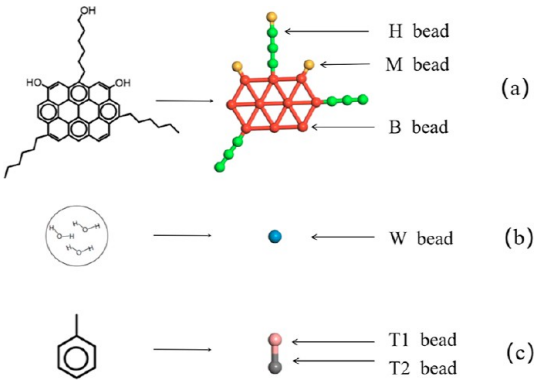

Figure 1. (a) Asphaltene coarse-grained model, (b) water coarse-grained model, and (c) toluene coarse-grained model (reproduced with permission from Ref Yosadara Ruiz-Morales, and Oliver C. Mullins. Copyright 2015. American Chemical Society).

2.3. DPD Parameters and Simulation Details. The DPD method is a coarse-grained simulation method in which the random force coefficient $\sigma = 3$, and the dissipative force coefficient $\eta = 4.5$ are controlled in the simulation, allowing the simulation to run at a temperature of $K_BT = 1$. The simulation applies periodic boundary conditions.[48,57,63−67] The degree of coarse graining used in here is $N_m = 3$. The volume of the beads is 90 Å^3, the radius of the beads is 6.46 Å, and the mass of the beads is 54 amu.[59,64,68] The equilibrium bond length r_0 = 3 Å and a spring constant of 300 kcal (mol·Å^2)$^{-1}$ are assigned for all the beads of aromatic rings.[31,32] The time scale τ is calculated by eq 13,[31,33,48] and the simulation scale τ = 3.0158 ps is calculated. The time step is set to 0.005τ, the number of kinetic simulation steps is 700,000, then an equilibrium simulation of 350,000 steps is performed, and the simulation is performed for a total of 15.08 ns. The time steps and simulation durations applied here are derived from the studies of Ruiz-Morales and Mullins.[31]

$$\tau = r_c\sqrt{m/k_BT} \tag{13}$$

The bead-to-bead interaction parameters are calculated with the method proposed by Groot and Warren.[69−71] The experimental Hansen solubility parameters and molar volumes are shown in Table 1,[31,68] and the conserved force parameters between the beads are shown in Table 2.

3. RESULTS AND DISCUSSION

3.1. Simulation Validation. Rezaei and Modarres et al.[45] experimentally calculated an interfacial tension of 36.11 mN/m for the toluene−water system. While Ruiz-Morales and Alvarez-Ramírez[48] obtained an IFT value of 45 mN/m for the toluene−water interface by DPD simulations, the calculated IFT here is not precisely compared with the reported experimental data, but the calculated IFT and the experimental data have the same order of magnitude. This is related to the number of water molecules in the beads, the volume of the beads, the cutoff distance, and the repulsion parameter (a_{ij}) between the beads. The IFT value calculated after the DPD simulation in this study is 44.268 mN/m, which is close to that calculated by Ruiz-Morales and Alvarez-Ramírez.[48]

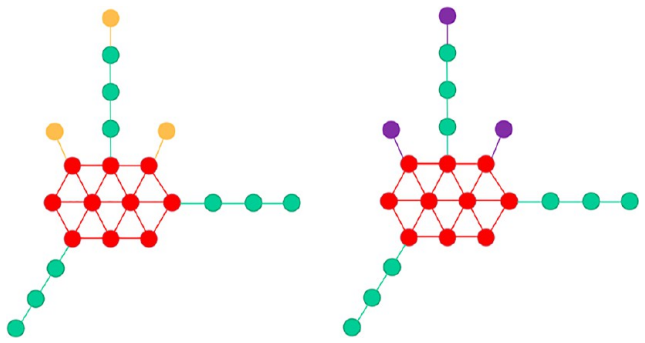

Figure 3. Different heteroatom type model asphaltenes (heteroatom types are oxygen-containing heteroatom M and non-oxygen-containing heteroatom T).

The interlayer distance can be calculated by the radial distribution function, and the first peak of the radial distribution function is conventionally taken as the interlayer distance value,[33,62,72] which is the distance between the first shell layers of asphaltene aggregation. The radial distribution function is calculated as follows[32,62]

$$g_{ij}(r) = \frac{\{\Delta N_{ij}(r \to r + \Delta r)\}V}{4\pi \cdot r^2 \Delta r N_i N_j} \tag{14}$$

where $\{\Delta N_{ij}(r \to r + \Delta r)\}$ represents the ensemble averaged number of j around i within a shell from r to $r + \Delta r$, V is the system volume, and NiNj are numbers of i and j, respectively.

The experimental value of the distance between the asphaltene molecular planes was in the range of 3−4 Å,[72] and the simulated value of the interlayer distance between asphaltenes after diffusion in the toluene solvent was calculated to be 3.05 Å, which is consistent with the experimental value. In Figure 6, the simulated calculated interlayer distances are within the experimental values, further demonstrating the accuracy of the DPD method to study the simulated system.

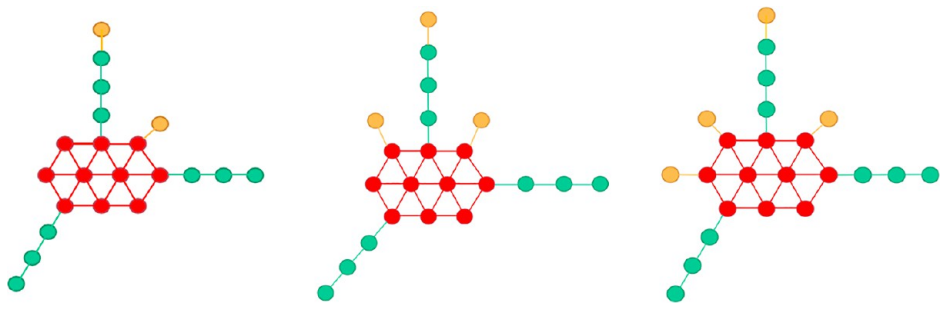

Figure 2. Model asphaltenes with different numbers of heteroatoms (2, 3, and 4 for the number of heteroatoms).

https://doi.org/10.1021/acsomega.3c05486
ACS Omega 2023, 8, 33083−33097

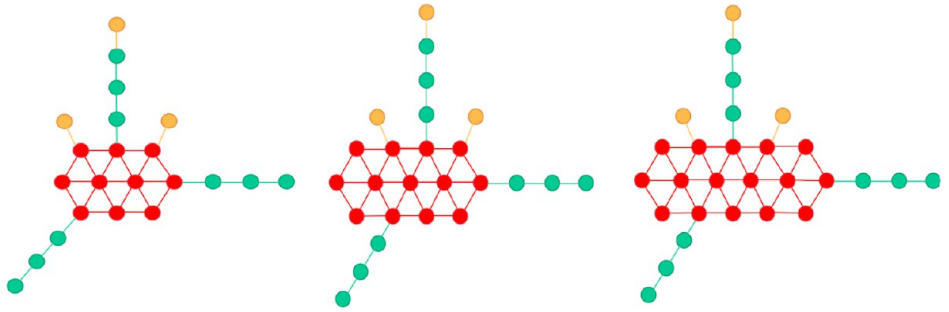

Figure 4. Model asphaltenes with different numbers of aromatic rings (10, 13, and 16 for the number of aromatic rings).

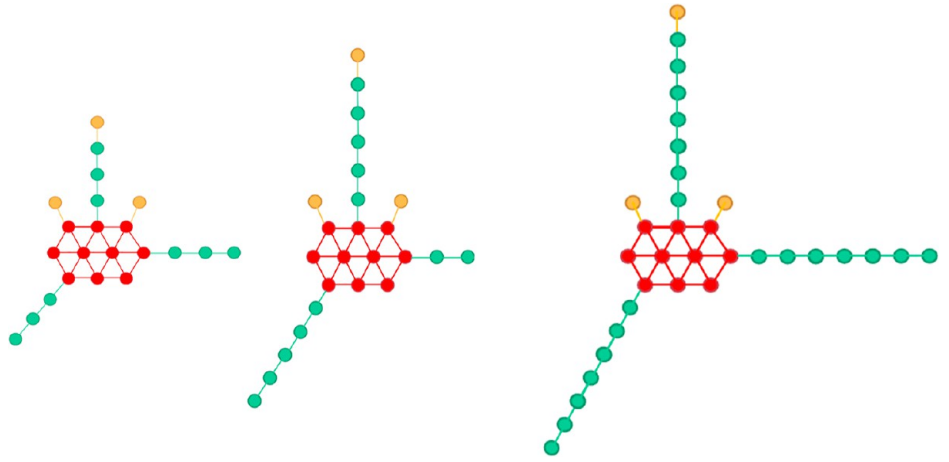

Figure 5. Model asphaltene molecules with different alkyl side-chain lengths (coarse granulation lengths of alkyl side chains are 3, 5, and 7, named T, F, and S, respectively).

Table 1. Experimental Hansen Solubility Parameters and Molar Volume

system	Hansen solubility parameter $(J/cm^3)^{1/2}$	molar volume (cm^3/mol)
oil	18.2	
toluene (T1, T2)	18.2	106.8
water (W)	47.9	18.0
benzene (B)	18.6	89.13
hexane (H)	14.9	131.6
methanol (M)	29.6	40.7
thiourea (T)	33.01	72.8

Table 2. Interaction Parameters between the Beads in the Simulated System

	B	H	T1	T2	W	M	T
B	25						
H	27	25					
T1	25	27	25				
T2	25	27	25	25			
W	90	140	103	103	25		
M	36	51	39	39	39	25	
T	49	72	53	53	39		25

The system is composed of asphaltene molecules solvated in oil and water. At the beginning of the simulation, the asphaltenes are randomly distributed in the oil phase. As the kinetic simulation proceeds, the asphaltene continuously moves toward the oil−water interface. The simulation proceeds to the 10 ns moment and the asphaltene is almost

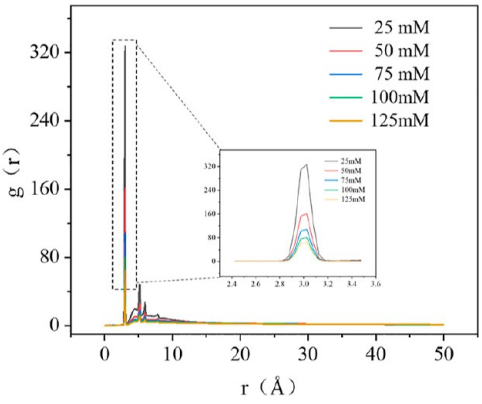

Figure 6. Radial distribution function of asphaltene in toluene at different concentrations.

completely adsorbed at the oil−water interface, as seen in the simulation snapshot in Figure 7. At the oil−water interface, the hydrophilic heteroatoms in the asphaltene enter the aqueous phase, while the hydrophobic alkyl side chains extend into the oil phase, as can be seen in Figure 8. The rigid structures of asphaltene polycyclic aromatic hydrocarbons (PAHs) show either horizontal adsorption at the oil−water interface or vertical or at an angle to the oil−water interface. This is in accordance with the study of Ruiz-Morales and Mullins.[31,48]

3.2. Effect of Asphaltene Structure. To investigate the effects of asphaltene structure on oil−water interfacial tension, we chose two typical asphaltene concentrations, 75 and 100 mM, for detailed analysis and discussion. The simulations

https://doi.org/10.1021/acsomega.3c05486
ACS Omega 2023, 8, 33083−33097

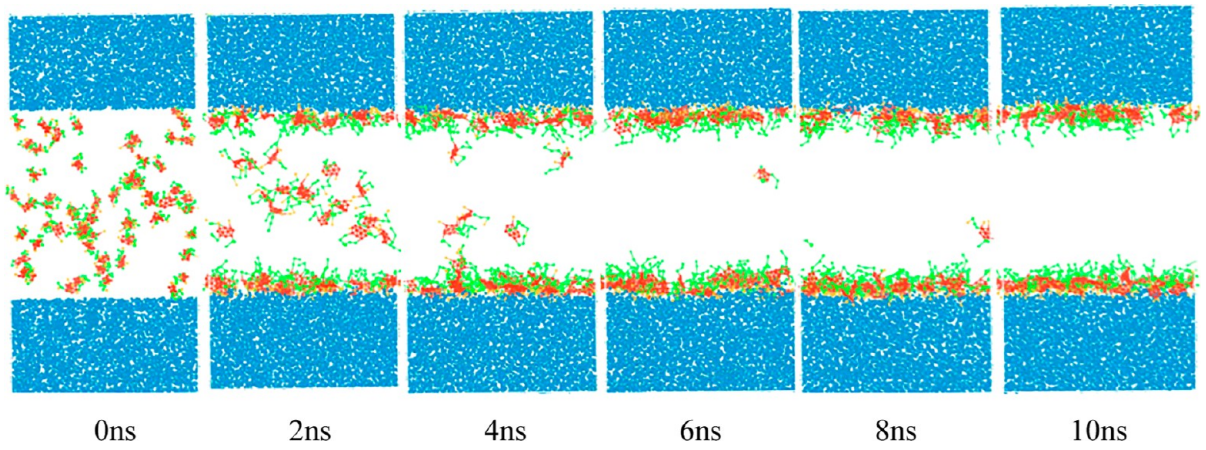

Figure 7. Movement of asphaltene in the system at different moments.

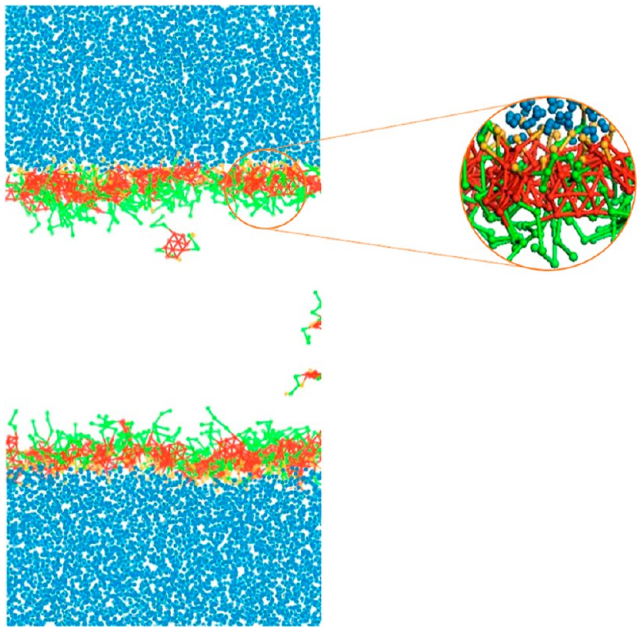

Figure 8. Detail of asphaltene adsorption at the oil−water interface.

demonstrated that these two concentrations effectively illustrate the behavior of asphaltene molecules in the system.

3.2.1. Effect of the Number of Asphaltene Heteroatoms. In order to explore the effect of different oxygen-containing heteroatoms on the properties of the oil−water interface, we set the number of heteroatoms in the modeled asphaltene to 2, 3, and 4. In other words, we are exploring how different numbers of heteroatoms affect the properties of the interface between oil and water. An increase in the number of heteroatoms implies an increase in the number of hydrophilic head groups. The increase in hydrophilic groups leads to an increase in asphaltene polarity, and asphaltene molecules are able to adsorb more firmly to the oil−water interface. As the number of heteroatoms in asphaltene molecules continues to increase, asphaltenes will play a greater role in reducing oil−water interfacial tension.

As can be seen from the simulation snapshot shown in Figure 9, asphaltenes possessing a higher number of heteroatoms are able to adsorb more at the oil−water interface at the same asphaltene concentration. The system has the same number of asphaltene molecules at the same concentration, and the system equilibrium contains four heteroatom asphaltene system has few free-form asphaltene molecules in

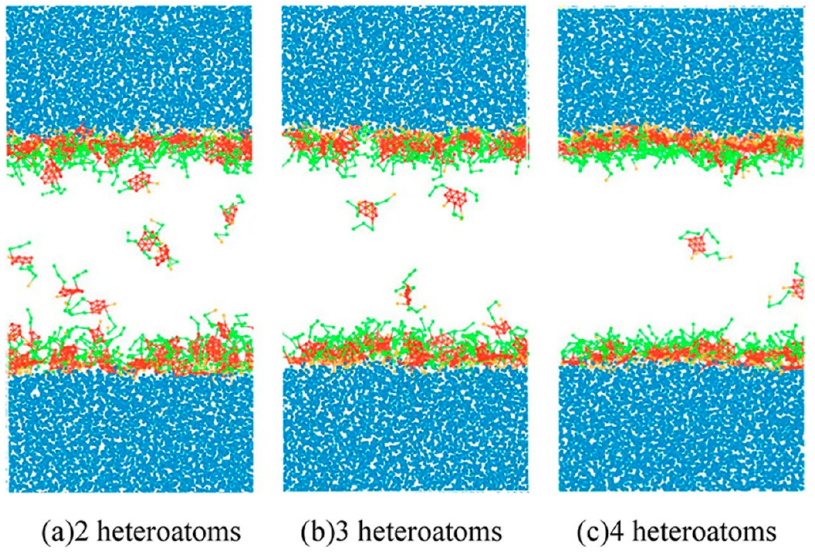

Figure 9. Equilibrium snapshots of asphaltene systems with different heteroatomic numbers at a concentration of 75 mM.

https://doi.org/10.1021/acsomega.3c05486
ACS Omega 2023, 8, 33083−33097

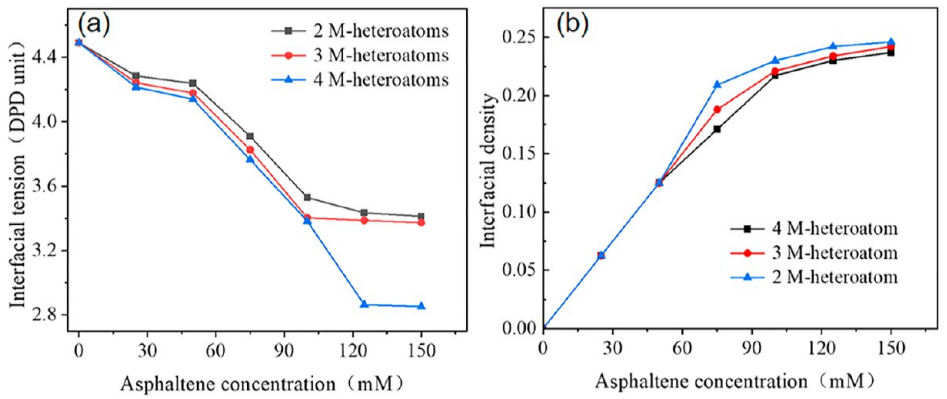

Figure 10. (a) Variation of asphaltene interfacial tension with the concentration of asphaltene system for different numbers of heteroatoms. (b) Variation of asphaltene interfacial density with the concentration of asphaltene system for different numbers of heteroatoms.

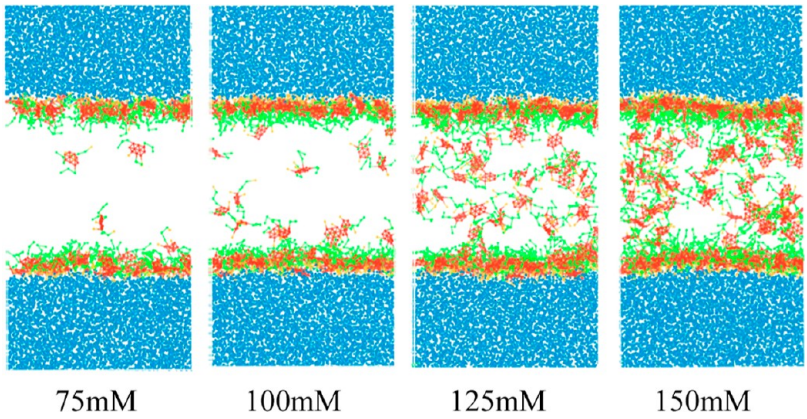

Figure 11. Equilibrium snapshot of asphaltene system behavior with the concentration in M heteroatomic asphaltene systems.

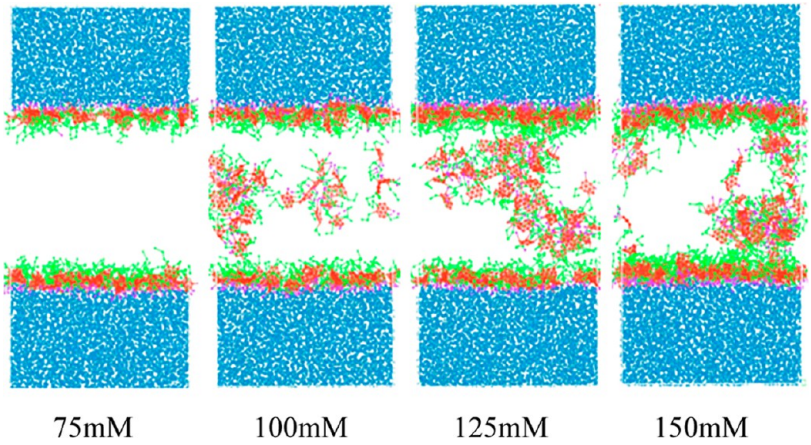

Figure 12. Equilibrium snapshot of asphaltene system behavior with a concentration in T heteroatomic asphaltene systems.

the oil phase, almost all of which are adsorbed at the oil−water interface. While asphaltene molecular systems containing two heteroatoms have more free-form asphaltene molecules in the oil phase, asphaltene systems containing three heteroatoms are in between. As shown in Figure 10b, the interfacial density of asphaltene molecules shows that for the same asphaltene concentration, the interfacial density is higher for asphaltenes with more heteroatoms in the system. As shown in Figure 10a, where the decreasing trend of interfacial tension is observed, as the number of heteroatoms in the asphaltene molecule increases, asphaltenes with more heteroatoms reduce the oil−water interfacial tension more than asphaltenes with fewer heteroatoms. This indicates that when the number of hydrophilic heteroatoms in asphaltene increases, asphaltene indicates that the active effect is enhanced, improving the ability of asphaltene to stabilize the oil−water interface.

3.2.2. Effect of Heteroatom Types. Asphaltenes containing different heteroatom types were arranged in the system, in which the heteroatom containing oxygen was named the M heteroatom and the heteroatom without oxygen was named T heteroatom. The effect of different types of heteroatoms on the interfacial properties was investigated by simulation. The

https://doi.org/10.1021/acsomega.3c05486
ACS Omega 2023, 8, 33083−33097

comparison shows that the role of T heteroatom asphaltenes and M heteroatom asphaltenes at the oil−water interface is different. The analysis of interfacial tension shows that T heteroatomic asphaltenes have higher interfacial activity and are more capable than M heteroatomic asphaltenes in reducing oil−water interfacial tension and stabilizing the interface (Figure 11).

In addition, we found that asphaltenes with T heteroatoms are more likely to form nanoaggregates. The free T-heteroatom asphaltenes in the oil phase form aggregates as can be seen in the simulation snapshot, as shown in Figure 12. It is related to the solubility of T-type heteroatomic asphaltenes in the oil phase of toluene. The T-type heteroatomic bitumen is more resistant to dissolution in toluene, which is why they can easily form aggregates in toluene. In contrast, M heteroatomic asphaltenes are more soluble in toluene than T heteroatomic asphaltenes; therefore, M heteroatomic asphaltenes are less likely to form aggregates in toluene. Mikami et al.[29] also found through their study that some asphaltenes form nanoaggregates. Rahmati[34] investigated the properties of asphaltene heteroatoms and alkyl side chains on their aggregation in aromatic solvents, and the results showed that asphaltene aggregation depends to a large extent on the type of heteroatoms in the asphaltene structure, and the conclusions obtained in this study are consistent with those obtained by previous authors.

In Figure 13, the slope of the MSD for two different types of heteroatomic asphaltene molecules in the oil−water system represents the diffusion rate of the two asphaltene molecules. The diffusion coefficients D, calculated from the slopes of the mean square displacements (MSD) in the long time limit using the following equation[62]

$$D = \frac{1}{2N_d} \lim_{t\to\infty} \frac{d}{dt} \sum_{i=1}^{N} [|r_i(t) - r_i(t)|^2] \quad (15)$$

where N_d is the dimensionality (N_d = 3 for the simulations) and $r_i(t)$ and $[|r_i(t) - r_i(0)|^2]$ are the position and squared displacement of given molecules at time t, respectively. Cheng and Yuan[73] found that asphaltenes are very important for the formation of emulsified oil droplets. Asphaltene polar groups can promote the diffusion of surfactants in oil droplets, while acidic asphaltene and surfactants will adsorb on the oil−water surface and form a water bridge structure with hydrogen bonds with water molecules, which makes the emulsion more stable. Wang et al.[25] concluded that when surface-active substances are present, it is generally assumed that the surface-active substances spontaneously diffuse and adsorb on the interfacial layer. This rate is greater than its self-diffusion rate in toluene solvent. Skartlien et al.[74] showed that the polar groups in asphaltene molecules enhance their adsorption capacity to the oil−water interface, and that their diffusion rate to the oil−water interface is enhanced by the pull of the polar groups. The rate of movement of asphaltenes in the oil−water system increases because the presence of hydrophilic heteroatoms of asphaltenes has an effect on their movement in the oil and water phases. It can be seen that the diffusion rate of T heteroatomic asphaltenes in the system is greater than that of M heteroatomic asphaltenes. This may be related to the fact that T heteroatomic asphaltene molecules are less soluble in the oil phase, and T heteroatomic asphaltenes repel more from the oil phase and move toward the oil−water interface at a faster rate in the presence of hydrophilic head groups. As a result, its diffusion rate in the system increases considerably and the slope of the MSD of the T heteroatom asphaltene increases.

As shown in Figure 14a, the variation law of interfacial tension with the concentration of asphaltene of the system was calculated for M heteroatom and T heteroatom asphaltenes, respectively. In Figure 14a, it can be seen that when the asphaltene concentration of the system is less than 80 mM, the effect of the two asphaltenes in reducing the interfacial tension is not much different, and the T heteroatomic asphaltene is

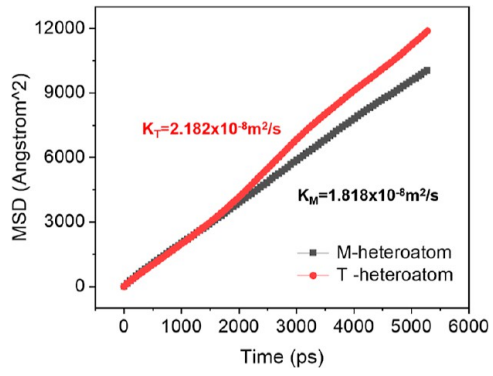

Figure 13. MSD of different kinds of heteroatomic asphaltenes in the system.

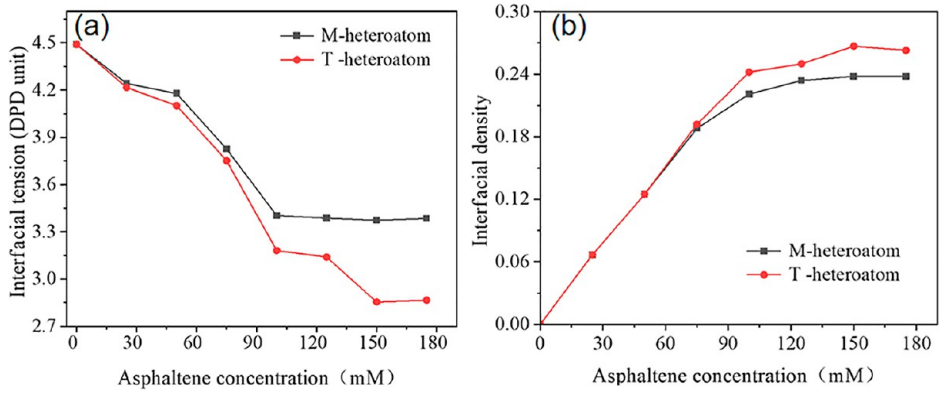

Figure 14. (a) Variation of interfacial tension of different types of heteroatomic asphaltenes with system concentration and (b) variation of interfacial density of different types of heteroatomic asphaltenes with system concentrations.

https://doi.org/10.1021/acsomega.3c05486
ACS Omega 2023, 8, 33083−33097

slightly better than the M heteroatomic asphaltene. At this point, the two heteroatomic asphaltene interfacial densities are almost the same, as shown in Figure 14b, which also proves that the T heteroatomic asphaltene interfacial activity is higher. When continuing to increase the asphaltene concentration of the system, T heteroatomic asphaltenes reduce the interfacial tension better than M heteroatomic asphaltenes. On the one hand, T heteroatomic asphaltenes have higher interfacial density than M heteroatomic asphaltenes, as shown in Figure 14b. On the other hand, this may have some relation with the formation of aggregates by T heteroatoms. As shown in Figure 15, the aggregates formed by T heteroatomic asphaltenes move to the oil−water interface film and cross-link with the oil−water interface asphaltene film layer, which may further reduce the oil−water interface tension. This document has discussed only the differences between heteroatomic groups of oxygen-containing elements and non-oxygen-containing heteroatomic groups of asphaltene molecules. Further research is needed to discuss the types and locations of heteroatomic groups in asphaltenes.

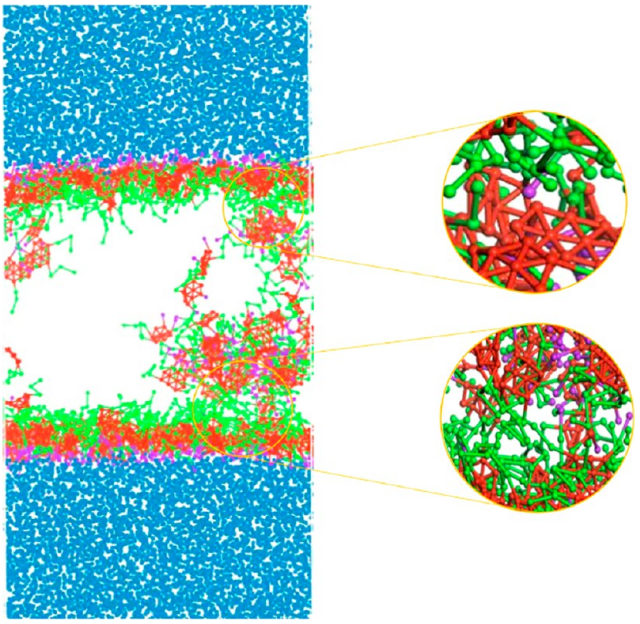

Figure 15. Simulated snapshot details of T heteroatom asphaltene system at a concentration of 150 mM.

3.2.3. Effect of the Number of Asphaltene Aromatic Rings. The number of aromatic rings of the model asphaltene was varied to study the effect of the number of aromatic rings on the properties of asphaltene at the oil−water interface. The model asphaltenes with aromatic ring numbers of 10, 13, and 16 were set up, respectively. Variation of the number of asphaltene aromatic rings affects the interfacial activity of the asphaltene and the interactions between asphaltene molecules. A higher number of aromatic rings can improve the coverage of asphaltene molecules at the oil−water interface and can better reduce the interfacial tension. Asphaltenes with more aromatic rings have stronger interactions with each other.

As shown in Figure 16, observation of a snapshot of an oil-asphalt-water simulation system with an asphaltene concentration of 75 mM shows that the number of free asphaltene molecules in the oil phase becomes increasing, while the amount of asphaltene adsorbed at the oil−water interface decreases as the number of aromatic rings increases. As the number of aromatic rings in asphaltene molecules increases, individual asphaltene molecules occupy a larger area, so that fewer amounts of asphaltene molecules are needed to cover the entire oil−water interface. The excessive number of asphaltene molecules leads to overcrowding at the oil−water interface; then, the amount of free asphaltene in the oil phase will increase. This situation is more clearly observed in the simulated snapshot of an asphaltene system concentration of 100 mM shown in Figure 17.

As shown in Figure 18, the oil−water interfacial tension decreases with the increase in the number of aromatic rings of asphaltenes, which indicates that asphaltenes with a higher number of aromatic rings are more effective in reducing interfacial tension. As shown in Figure 19, the asphaltene−asphaltene RDF peak rose as the number of aromatic rings in asphaltenes increased, which proves that asphaltenes with a

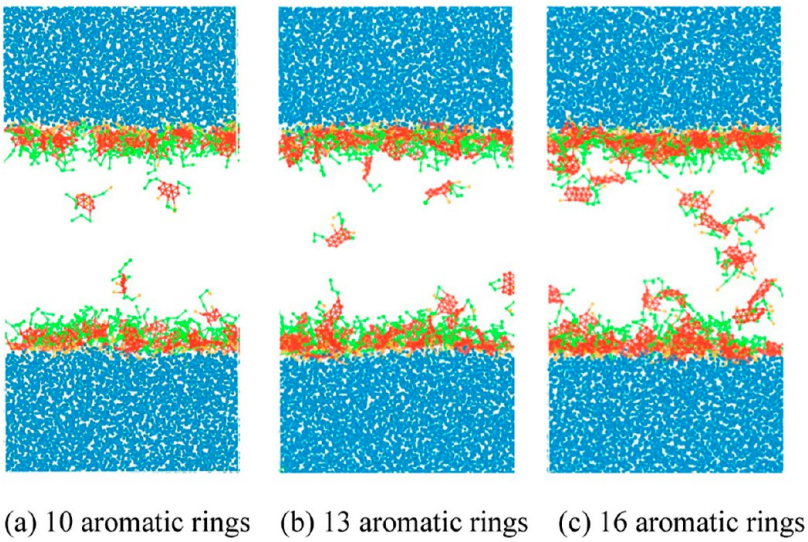

Figure 16. Equilibrium snapshots of asphaltene systems with different numbers of aromatic rings at a concentration of 75 mM (a) 10 aromatic rings, (b) 13 aromatic rings, and (c) 16 aromatic rings.

https://doi.org/10.1021/acsomega.3c05486
ACS Omega 2023, 8, 33083−33097

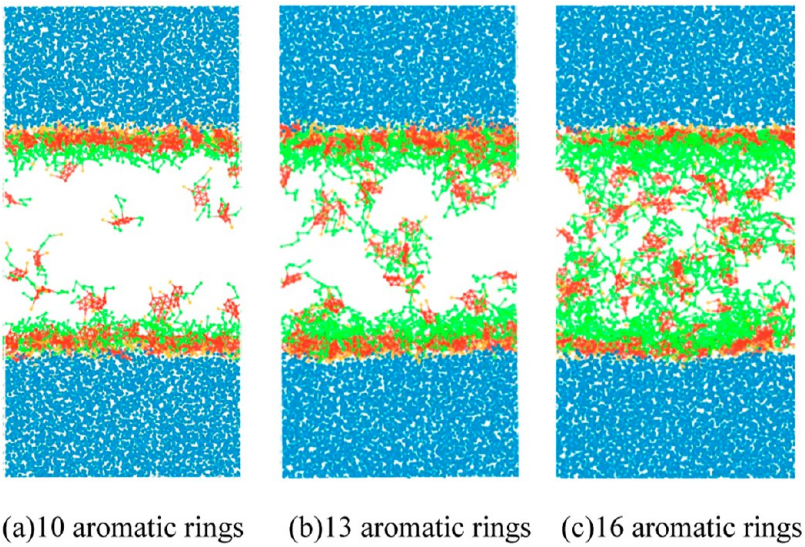

Figure 17. Equilibrium snapshots of asphaltene systems with different numbers of aromatic rings at a concentration of 100 mM (a) 10 aromatic rings, (b) 13 aromatic rings, and (c) 16 aromatic rings.

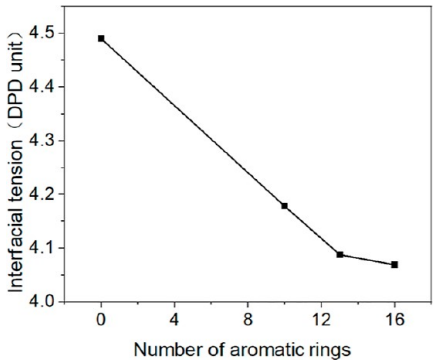

Figure 18. Variation of interfacial tension with the asphaltene aromatic ring number.

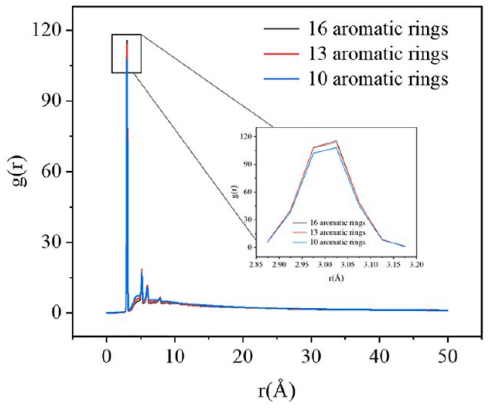

Figure 19. Asphaltene−asphaltene radial distribution function for different aromatic ring numbers.

high number of aromatic rings have a stronger aggregation ability and stronger interactions between asphaltene molecules. It also indicates that the interfacial film formed by asphaltene molecules with a high number of aromatic rings is more stable. Sedghi et al.[37] also demonstrated in their simulations that the strength of the interaction between asphaltene PAHs is the driving force for the association, and the strength of driving force depends on the number of aromatic rings.

As shown in Figure 20b, the asphaltene interfacial density gradually decreases with the increase of the number of aromatic rings. Because the number of aromatic rings becomes larger, the asphaltenes adsorbed at the oil−water interface occupy a larger interfacial area and squeeze the excess asphaltenes into the oil phase. When the asphaltene concentration of the system is less than 75 mM, the oil−water interface is not yet saturated with adsorption and at this time, the three structures of asphaltene density is approximately the same. At this time, the interfacial tension of all three structural asphaltenes decreased with increasing concentration, and the asphaltenes with an aromatic ring number of 16 were more capable of reducing the interfacial tension, followed by those with an aromatic ring number of 13, and those with an aromatic ring number of 10 were the least capable of reducing the interfacial tension, as shown in Figure 20a. When the number of asphaltene molecules adsorbed at the interface is the same, the asphaltene with more aromatic rings covers a larger area and has a stronger association between asphaltene molecules, which can reduce the interfacial tension more efficiently.

When the asphaltene concentration of the system is in the range of 75 and 100 mM, the interfacial stability may be jointly determined by the number of asphaltene interfacial adsorption, the asphaltene interfacial coverage area and the strength of the interaction between asphaltene molecules, when the effect of the three asphaltene molecules in reducing the interfacial tension is basically the same. When the asphaltene concentration of the system is greater than 100 mM, asphaltenes with a higher number of aromatic rings are effective in reducing interfacial tension. Although asphaltenes with a higher number of aromatic rings have a less amount of interfacial adsorption, the higher number of aromatic rings of asphaltene molecules leads to a larger molecular coverage area, while the associative effect between asphaltene molecules with a higher number of aromatic rings is stronger.

The results demonstrated that the magnitude of the oil−water interfacial tension of asphaltenes with different aromatic ring numbers is influenced by three main factors. The first

https://doi.org/10.1021/acsomega.3c05486
ACS Omega 2023, 8, 33083−33097

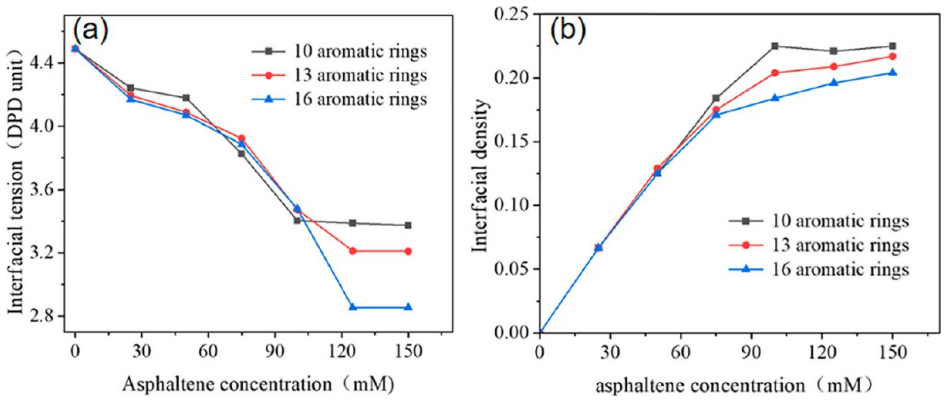

Figure 20. (a) Variation of interfacial tension of asphaltenes with different numbers of aromatic ring nuclei with the concentration of asphaltenes in the system and (b) variation of interfacial density of asphaltenes with different numbers of aromatic ring nuclei with the concentration of asphaltenes in the system.

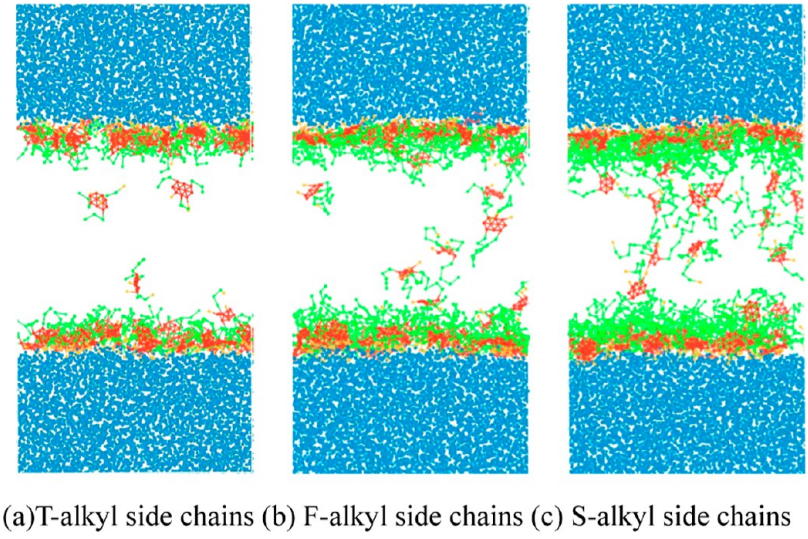

Figure 21. Effect of asphaltene alkyl side-chain length on the interface at a concentration of 75 mM (a) T-alkyl side chains, (b) F-alkyl side chains, and (c) S-alkyl side chains.

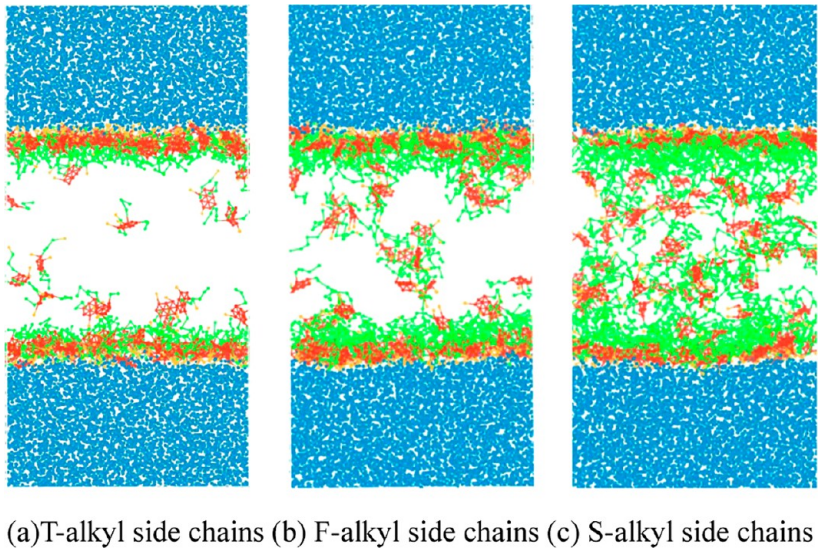

Figure 22. Effect of asphaltene alkyl side-chain length on the interface at a concentration of 100 mM (a) T-alkyl side chains, (b) F-alkyl side chains, and (c) S-alkyl side chains.

https://doi.org/10.1021/acsomega.3c05486
ACS Omega 2023, 8, 33083−33097

factor is the amount of asphaltene adsorbed at the oil−water interface. As the amount of asphaltene adsorbed at the interface increases, the oil−water interfacial tension decreases, which is a factor affecting the magnitude of interfacial tension. Second, the number of aromatic rings of asphaltene molecules increases the interfacial area occupied by them, and their effect of reducing interfacial tension is improved. The third factor is that asphaltene molecules with a high number of aromatic rings have a stronger association with each other and form a more stable interfacial film.

3.2.4. Effect of Asphaltene Alkyl Side-Chain Length. The lengths of asphaltene alkyl side chains were changed to set the alkyl side-chain coarse granulation lengths of 3, 5, and 7 bead lengths, and the side chains with coarse granulation degrees of 3, 5, and 7 were named T, F, and S alkyl side chains, respectively. The length of asphaltene alkyl side chains has been found to have an effect on asphaltene adsorption at the oil−water interface through simulation studies. Because different alkyl side chains have various solubilities for the oil phase, asphaltenes with different alkyl side-chain lengths will interact varyingly with the oil and water phases of the system, while various interactions will occur between asphaltene molecules. The longer alkyl side-chains of asphaltenes can extend more firmly into the oil phase, and the long chains make the structure of the formed interfacial film more complex. However, the complex interfacial film structure formed prevents further adsorption of asphaltenes from the oil phase to the oil−water interface. Rahmati et al. found through molecular dynamics studies that increasing the length of alkyl side chains on the asphaltene structure prevents the aromatic rings in the asphaltene from moving toward each other. As shown in Figures 21 and 22, as the length of asphaltene alkyl side chains continues to increase, the amount of free asphaltene blocked outside the dense interfacial film increases with the length of alkyl side chains. The formation of denser interfacial films by long alkyl side chains as well as the spatial site resistance effect of long chains further hinder the adsorption of asphaltenes at the oil−water interface. Jian et al.[36] investigated the effect of side-chain length on the aggregation of model asphaltenes by molecular dynamics and found that longer alkyl side chains hinder the stacking of parallel structures of asphaltene aromatic nuclei. The results obtained in this study are consistent with others regarding the phenomenon that long alkyl side chains hinder asphaltene adsorption to the oil−water interface.

As shown in Figure 23, observing the asphaltene relative concentration distribution for a system concentration of 100 mM shows that the width of the peak of the asphaltene relative concentration distribution increases with the increase of the length of the asphaltene alkyl side chain, which indicates that the interfacial film thickness is increasing. The peaks in the asphaltene relative concentration distribution plot decrease sequentially with increasing length of the alkyl side chains. The explanation is that while the longer alkyl side chains of the asphaltene molecules make the interfacial film more intensive, the spatial barrier effect of the longer chains prevents the asphaltene molecules from continuing to adsorb to the oil−water interface and the quantity of free-form asphaltene molecules in the oil phase is increased. As shown in Figure 24, the RDF peak between asphaltene molecules increases with the increase of alkyl side chains, which proves that short alkyl side-chain asphaltene molecules have a greater attraction between each other and their molecular interactions are stronger.

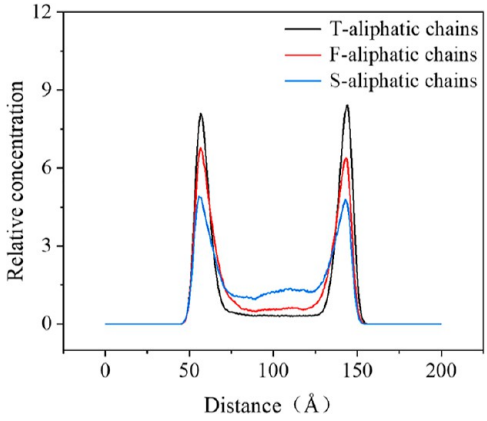

Figure 23. Relative concentration distribution in asphaltene systems with different alkyl side-chain lengths at a concentration of 100 mM.

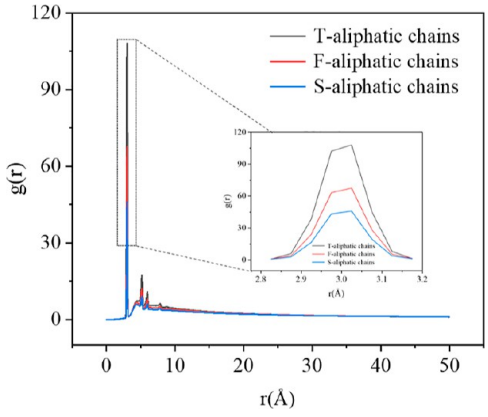

Figure 24. Asphaltene−asphaltene radial distribution function for different alkyl side-chain lengths.

The thickness of the interfacial film between the oil−water interface was observed to improve as the length of the alkyl side chains of the asphaltene molecules increased and the interaction forces between the longer alkyl side-chain asphaltene molecules decreased. At the same time, the asphaltene molecules adsorbed at the oil−water interface decreased as the alkyl side-chain length increased. The simulation research found that F alkyl side-chain asphaltene molecules decreased the interfacial tension better than T and S alkyl side-chain asphaltene molecules, and the change of asphaltene alkyl side-chain length was non-monotonic with the interfacial tension reduction effect, as shown in Figure 25.

Observation of the variation in interfacial tension in Figure 25 revealed that all three alkyl side-chain lengths of asphaltenes were effective in reducing interfacial tension as the concentration of asphaltenes in the system continued to increase. For T-alkyl side-chain asphaltene molecules, the interfacial tension no longer decreases after continuing to increase the asphaltene concentration when the concentration reaches 100 mM. For the F and S alkyl side-chain asphaltene molecules, the interfacial tension also decreases when the asphaltene concentration continues to increase and when the system concentration reaches 125 mM, the interfacial tension almost ceases to change. Although the interfacial film formed by longer alkyl side-chain asphaltenes is thicker, F alkyl side-chain asphaltenes reduce the interfacial tension better than S alkyl side-chain asphaltenes because more F alkyl side-chain asphaltenes are adsorbed at the oil−water interface than S alkyl

https://doi.org/10.1021/acsomega.3c05486
ACS Omega 2023, 8, 33083−33097

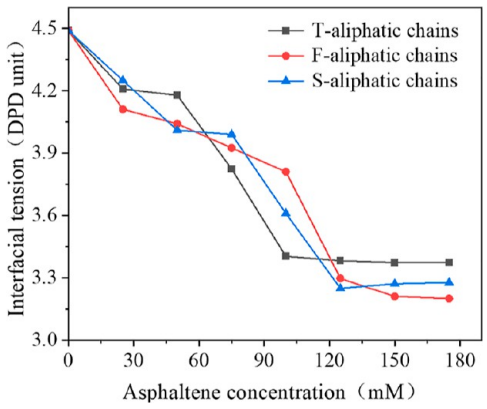

Figure 25. Variation of interfacial tension of asphaltenes with different alkyl side-chain structures with asphaltene system concentrations.

side-chain asphaltenes, and the interaction force between F alkyl side-chain asphaltenes molecules is stronger. Such medium-length asphaltene molecules combine the advantages of both, resulting in the best reduction of interfacial tension. The magnitude of interfacial tension depends on the number of interfacial asphaltene molecules, the thickness of the asphaltene interfacial film, and the interactions between asphaltene molecules. These factors determine the strength of the oil-water interfacial film, which is the reason why the interfacial tension variation is not monotonic with the alkyl side-chain length variation.

4. CONCLUSIONS

The conclusions can be drawn from simulation studies of dissipative particle dynamics. Asphaltene will diffuse to the oil−water interface due to its own surface activity and form an interfacial film at the oil−water interface, which can effectively reduce the interfacial tension and enhance the stability of the oil−water interface. As the asphaltene concentration in the system increases, the asphaltene will continue to adsorb to the oil−water interface, while the thickness of the interfacial film increases. As the interfacial film increases to a certain point, asphaltenes continue to be added, asphaltenes are not continually adsorbed to the interfacial film, the thickness of the interfacial film no longer increases, and the interfacial tension is not further reduced.

Research shows that increasing the number of heteroatoms in asphaltenes can effectively increase the interfacial activity of asphaltenes. When asphaltene molecules have more hydrophilic heteroatoms, the asphaltene has a greater interfacial adsorption capacity, while the asphaltene molecules can reduce interfacial tension more effectively. The type of heteroatom in the asphaltene also affects the behavior of the asphaltene. It was found that asphaltenes with non-oxygenated heteroatoms can reduce interfacial tension more effectively, while asphaltenes with non-oxygenated heteroatoms are more likely to form aggregates in the oil phase compared to asphaltenes with oxygen-containing heteroatoms.

Asphaltenes with a higher number of aromatic rings have a larger adsorption area at the oil−water interface and stronger intermolecular interactions between asphaltenes. Asphaltene molecules are capable of reducing interfacial tension more effectively as the number of aromatic rings in the asphaltene molecule is increased, and their capacity to reduce interfacial tension is enhanced as the number of aromatic rings in the asphaltene increases.

While increasing the length of the alkyl side chains can effectively improve the thickness of the interfacial film formed by asphaltenes, the longer alkyl side chains can impede the adsorption of asphaltene molecules at the oil−water interface. Research has revealed stronger interactions between short alkyl side-chain asphaltene molecules. The variations of oil−water interfacial tension are not monotonic with the composition of the alkyl side-chain length. Asphaltene molecules of medium length have the strongest ability to reduce interfacial tension, and long alkyl side-chain asphaltenes are more capable of reducing oil−water interfacial tension compared to short alkyl side-chain asphaltenes.

AUTHOR INFORMATION

Corresponding Author

Xiaoyan Liu − *School of Mechanical Science and Engineering, Northeast Petroleum University, Daqing 163318, China*; Email: liu_xydq@163.com

Authors

Chonghao Liang − *School of Mechanical Science and Engineering, Northeast Petroleum University, Daqing 163318, China*; orcid.org/0009-0000-9666-719X

Hui Jiang − *School of Civil Architecture and Engineering, Northeast Petroleum University, Daqing 163318, China*

Ying Xu − *School of Mechanical Science and Engineering, Northeast Petroleum University, Daqing 163318, China*

Yongying Jia − *School of Mechanical Science and Engineering, Northeast Petroleum University, Daqing 163318, China*

Complete contact information is available at: https://pubs.acs.org/10.1021/acsomega.3c05486

Notes

The authors declare no competing financial interest.

ACKNOWLEDGMENTS

This work was supported by the National Natural Science Foundation of China (52076036) and the Natural Science Foundation of Heilongjiang Province of China (LH2020E017).

REFERENCES

(1) Kilpatrick, P. K. Water-in-Crude Oil Emulsion Stabilization: Review and Unanswered Questions. *Energy Fuels* **2012**, *26*, 4017−4026.

(2) Gafonova, O. V.; Yarranton, H. W. The Stabilization of Water-in-Hydrocarbon Emulsions by Asphaltenes and Resins. *J. Colloid Interface Sci.* **2001**, *241*, 469−478.

(3) Harbottle, D.; Chen, Q.; Moorthy, K.; Wang, L.; Xu, S.; Liu, Q.; Sjoblom, J.; Xu, Z. Problematic stabilizing films in petroleum emulsions: shear rheological response of viscoelastic asphaltene films and the effect on drop coalescence. *Langmuir* **2014**, *30*, 6730−6738.

(4) Yang, F.; Tchoukov, P.; Pensini, E.; Dabros, T.; Czarnecki, J.; Masliyah, J.; Xu, Z. Asphaltene Subfractions Responsible for Stabilizing Water-in-Crude Oil Emulsions. Part 1: Interfacial Behaviors. *Energy Fuels* **2014**, *28*, 6897−6904.

(5) Fan, Y.; Simon, S.; Sjöblom, J. Interfacial shear rheology of asphaltenes at oil−water interface and its relation to emulsion stability: Influence of concentration, solvent aromaticity and nonionic surfactant. *Colloids Surf., A* **2010**, *366*, 120−128.

(6) Nenningsland, A. L.; Gao, B.; Simon, S.; Sjöblom, J. Comparative Study of Stabilizing Agents for Water-in-Oil Emulsions. *Energy Fuels* **2011**, *25*, 5746−5754.
(7) Tchoukov, P.; Yang, F.; Xu, Z.; Dabros, T.; Czarnecki, J.; Sjoblom, J. Role of asphaltenes in stabilizing thin liquid emulsion films. *Langmuir* **2014**, *30*, 3024−3033.
(8) Rahham, Y.; Rane, K.; Goual, L. Characterization of the Interfacial Material in Asphaltenes Responsible for Oil/Water Emulsion Stability. *Energy Fuels* **2020**, *34*, 13871−13882.
(9) Song, G.; Ning, Y.; Li, Y.; Wang, W. Investigation on hydrate growth at the oil−water interface: In the presence of asphaltene. *Chin. J. Chem. Eng.* **2022**, *45*, 211−218.
(10) Sodero, A. C. R.; Santos Silva, H.; Guevara Level, P.; Bouyssiere, B.; Korb, J.-P.; Carrier, H.; Alfarra, A.; Bégué, D.; Baraille, I. Investigation of the Effect of Sulfur Heteroatom on Asphaltene Aggregation. *Energy Fuels* **2016**, *30*, 4758−4766.
(11) Santos Silva, H.; Alfarra, A.; Vallverdu, G.; Bégué, D.; Bouyssiere, B.; Baraille, I. Asphaltene aggregation studied by molecular dynamics simulations: role of the molecular architecture and solvents on the supramolecular or colloidal behavior. *Petrol. Sci.* **2019**, *16*, 669−684.
(12) Wang, S.; Xu, J.; Wen, H. The aggregation and diffusion of asphaltenes studied by GPU-accelerated dissipative particle dynamics. *Comput. Phys. Commun.* **2014**, *185*, 3069−3078.
(13) Mullins, O. C. The Modified Yen Model. *Energy Fuels* **2010**, *24*, 2179−2207.
(14) Mullins, O. C.; Sabbah, H.; Eyssautier, J.; Pomerantz, A. E.; Barré, L.; Andrews, A. B.; Ruiz-Morales, Y.; Mostowfi, F.; McFarlane, R.; Goual, L.; Lepkowicz, R.; Cooper, T.; Orbulescu, J.; Leblanc, R. M.; Edwards, J.; Zare, R. N. Advances in Asphaltene Science and the Yen−Mullins Model. *Energy Fuels* **2012**, *26*, 3986−4003.
(15) Zhang, S.; Zhang, L.; Lu, X.; Shi, C.; Tang, T.; Wang, X.; Huang, Q.; Zeng, H. Adsorption kinetics of asphaltenes at oil/water interface: Effects of concentration and temperature. *Fuel* **2018**, *212*, 387−394.
(16) Zarkar, S.; Pauchard, V.; Farooq, U.; Couzis, A.; Banerjee, S. Interfacial Properties of Asphaltenes at Toluene−Water Interfaces. *Langmuir* **2015**, *31*, 4878−4886.
(17) Liu, D.; Li, C.; Zhang, X.; Yang, F.; Sun, G.; Yao, B.; Zhang, H. Polarity effects of asphaltene subfractions on the stability and interfacial properties of water-in-model oil emulsions. *Fuel* **2020**, *269*, 117450.
(18) Xie, L.; Lu, Q.; Tan, X.; Liu, Q.; Tang, T.; Zeng, H. Interfacial behavior and interaction mechanism of pentol/water interface stabilized with asphaltenes. *J. Colloid Interface Sci.* **2019**, *553*, 341−349.
(19) Alves, C. A.; Romero Yanes, J. F.; Feitosa, F. X.; de Sant'Ana, H. B. Influence of asphaltenes and resins on water/model oil interfacial tension and emulsion behavior: Comparison of extracted fractions from crude oils with different asphaltene stability. *J. Petrol. Sci. Eng.* **2022**, *208*, 109268.
(20) Zhang, Y.; Fang, S.; Tao, T.; Xiong, Y.; Duan, M. Influence of Asphaltene Concentration on the Interfacial Properties of Two Typical Demulsifiers. *J. Dispersion Sci. Technol.* **2015**, *37*, 1453−1459.
(21) You, J.; Li, C.; Liu, D.; Yang, F.; Sun, G. Influence of the Aggregation State of Asphaltenes on Structural Properties of the Model Oil/Brine Interface. *Energy Fuels* **2019**, *33*, 2994−3002.
(22) Orbulescu, J.; Mullins, O. C.; Leblanc, R. M. Surface Chemistry and Spectroscopy of UG8 Asphaltene Langmuir Film, Part 2. *Langmuir* **2010**, *26*, 15265−15271.
(23) Feng, X.; Mussone, P.; Gao, S.; Wang, S.; Wu, S.-Y.; Masliyah, J. H.; Xu, Z. Mechanistic Study on Demulsification of Water-in-Diluted Bitumen Emulsions by Ethylcellulose. *Langmuir* **2009**, *26*, 3050−3057.
(24) Larichev, Y. V.; Nartova, A. V.; Martyanov, O. N. The influence of different organic solvents on the size and shape of asphaltene aggregates studied via small-angle X-ray scattering and scanning tunneling microscopy. *Adsorpt. Sci. Technol.* **2016**, *34*, 244−257.
(25) Wang, Y.; Cheng, T.; Zhou, G. Study on the Mechanism of Asphaltenes Reducing Oil-Water Interfacial Tension. *Chem. Res. Chin. Univ.* **2021**, *38*, 616−621.
(26) You, J.; Li, C.; Liu, D.; Yang, F.; Sun, G. Influence of the Aggregation State of Asphaltenes on Structural Properties of the Model Oil/Brine Interface. *Energy Fuels* **2019**, *33*, 2994−3002.
(27) Cagna, A.; Esposito, G.; Quinquis, A.-S.; Langevin, D. On the reversibility of asphaltene adsorption at oil-water interfaces. *Colloids Surf., A* **2018**, *548*, 46−53.
(28) Ma, J.; Yang, Y.; Li, X.; Sui, H.; He, L. Mechanisms on the stability and instability of water-in-oil emulsion stabilized by interfacially active asphaltenes: Role of hydrogen bonding reconstructing. *Fuel* **2021**, *297*, 120763.
(29) Mikami, Y.; Liang, Y.; Matsuoka, T.; Boek, E. S. Molecular Dynamics Simulations of Asphaltenes at the Oil−Water Interface: From Nanoaggregation to Thin-Film Formation. *Energy Fuels* **2013**, *27*, 1838−1845.
(30) Jian, C.; Poopari, M. R.; Liu, Q.; Zerpa, N.; Zeng, H.; Tang, T. Reduction of Water/Oil Interfacial Tension by Model Asphaltenes: The Governing Role of Surface Concentration. *J. Phys. Chem. B* **2016**, *120*, 5646−5654.
(31) Ruiz-Morales, Y.; Mullins, O. C. Coarse-Grained Molecular Simulations to Investigate Asphaltenes at the Oil−Water Interface. *Energy Fuels* **2015**, *29*, 1597−1609.
(32) Chen, J.; Chen, J.; Zhong, C.; Chen, S.; Chen, B.; Fang, S.; Xiang, W. Mesoscopic probes in asphaltenes nanoaggregate structure: from perpendicular to paralleled orientation at the water-in-oil emulsions interface. *RSC Adv.* **2017**, *7*, 38193−38203.
(33) de Oliveira, F. C.; Maia, J. M.; Tavares, F. W. Asphaltenes at the water-oil interface using DPD/COSMO-SAC. *Colloids Surf., A* **2021**, *625*, 126828.
(34) Rahmati, M. Effects of heteroatom and aliphatic chains of asphaltene molecules on their aggregation properties in aromatics Solvents: A molecular dynamics simulation study. *Chem. Phys. Lett.* **2021**, *779*, 138847.
(35) Kuznicki, T.; Masliyah, J. H.; Bhattacharjee, S. Aggregation and Partitioning of Model Asphaltenes at Toluene−Water Interfaces: Molecular Dynamics Simulations. *Energy Fuels* **2009**, *23*, 5027−5035.
(36) Jian, C.; Tang, T.; Bhattacharjee, S. Probing the Effect of Side-Chain Length on the Aggregation of a Model Asphaltene Using Molecular Dynamics Simulations. *Energy Fuels* **2013**, *27*, 2057−2067.
(37) Sedghi, M.; Goual, L.; Welch, W.; Kubelka, J. Effect of Asphaltene Structure on Association and Aggregation Using Molecular Dynamics. *J. Phys. Chem. B* **2013**, *117*, 5765−5776.
(38) Silva, H. S.; Sodero, A. C. R.; Bouyssiere, B.; Carrier, H.; Korb, J.-P.; Alfarra, A.; Vallverdu, G.; Bégué, D.; Baraille, I. Molecular Dynamics Study of Nanoaggregation in Asphaltene Mixtures: Effects of the N, O, and S Heteroatoms. *Energy Fuels* **2016**, *30*, 5656−5664.
(39) Ruiz-Morales, Y.; Alvarez-Ramirez, F. Usage of the Y-Rule and the Effect of the Occurrence of Heteroatoms (N, S) on the Frontier Molecular Orbitals Gap of Polycyclic Aromatic Hydrocarbons (PAHs), and Asphaltene-PAHs. *ChemPhysChem* **2023**, *24*, No. e202200682.
(40) Ruiz-Morales, Y. Application of the Y-Rule and Theoretical Study to Understand the Topological and Electronic Structures of Polycyclic Aromatic Hydrocarbons from Atomic Force Microscopy Images of Soot, Coal Asphaltenes, and Petroleum Asphaltenes. *Energy Fuels* **2022**, *36*, 8725−8748.
(41) Tirjoo, A.; Bayati, B.; Rezaei, H.; Rahmati, M. Molecular dynamics simulations of asphaltene aggregation under different conditions. *J. Petrol. Sci. Eng.* **2019**, *177*, 392−402.
(42) Derakhshani-Molayousefi, M.; McCullagh, M. Deterring Effect of Resins on the Aggregation of Asphaltenes in n-Heptane. *Energy Fuels* **2020**, *34*, 16081−16088.
(43) Wang, S.; Yang, S.; Wang, R.; Tian, R.; Zhang, X.; Sun, Q.; Liu, L. Dissipative particle dynamics study on the temperature dependent interfacial tension in surfactant-oil-water mixtures. *J. Petrol. Sci. Eng.* **2018**, *169*, 81−95.

https://doi.org/10.1021/acsomega.3c05486
ACS Omega 2023, 8, 33083−33097

(44) Wang, S.; Yang, S.; Wang, X.; Liu, Y.; Yang, S.; Dong, Q. Numerical simulations of the effect of ionic surfactant/polymer on oil-water interface using dissipative particle dynamics. *Asia-Pac. J. Chem. Eng.* **2016**, *11*, 581−593.
(45) Rezaei, H.; Modarress, H. Dissipative particle dynamics (DPD) study of hydrocarbon−water interfacial tension (IFT). *Chem. Phys. Lett.* **2015**, *620*, 114−122.
(46) Li, Y.; Zhang, H.; Bao, M.; Wang, Z. Dissipative particle dynamics simulation on the association between polymer and surfactant: Effects of surfactant and polymer feature. *Comput. Mater. Sci.* **2012**, *63*, 154−162.
(47) Li, Y.; Guo, Y.; Xu, G.; Wang, Z.; Bao, M.; Sun, N. Dissipative particle dynamics simulation on the properties of the oil/water/surfactant system in the absence and presence of polymer. *Mol. Simul.* **2013**, *39*, 299−308.
(48) Ruiz-Morales, Y.; Alvarez-Ramírez, F. Mesoscale Dissipative Particle Dynamics to Investigate Oil Asphaltenes and Sodium Naphthenates at the Oil−Water Interface. *Energy Fuels* **2021**, *35*, 9294−9311.
(49) Hoogerbrugge, P.; Koelman, J. Simulating Microscopic Hydrodynamic Phenomena with Dissipative Particle Dynamics. *Europhys. Lett.* **1992**, *19*, 155−160.
(50) Ginzburg, V. V.; Chang, K.; Jog, P. K.; Argenton, A. B.; Rakesh, L. Modeling the interfacial tension in oil-water-nonionic surfactant mixtures using dissipative particle dynamics and self-consistent field theory. *J. Phys. Chem. B* **2011**, *115*, 4654−4661.
(51) Vo, M. D.; Shiau, B.; Harwell, J. H.; Papavassiliou, D. V. Adsorption of anionic and non-ionic surfactants on carbon nanotubes in water with dissipative particle dynamics simulation. *J. Chem. Phys.* **2016**, *144*, 204701.
(52) Alasiri, H.; Chapman, W. G. Dissipative particle dynamics (DPD) study of the interfacial tension for alkane/water systems by using COSMO-RS to calculate interaction parameters. *J. Mol. Liq.* **2017**, *246*, 131−139.
(53) Shi, K.; Lian, C.; Bai, Z.; Zhao, S.; Liu, H. Dissipative particle dynamics study of the water/benzene/caprolactam system in the absence or presence of non-ionic surfactants. *Chem. Eng. Sci.* **2015**, *122*, 185−196.
(54) Liang, X.; Wu, J.; Yang, X.; Tu, Z.; Wang, Y. Investigation of oil-in-water emulsion stability with relevant interfacial characteristics simulated by dissipative particle dynamics. *Colloids Surf., A* **2018**, *546*, 107−114.
(55) Song, X.; Shi, P.; Duan, M.; Fang, S.; Ma, Y. Investigation of demulsification efficiency in water-in-crude oil emulsions using dissipative particle dynamics. *RSC Adv.* **2015**, *5*, 62971−62981.
(56) Hu, C.; Liu, S.; Fang, S.; Xiang, W.; Duan, M. Dissipative particle dynamics investigation of demulsification process and mechanism of comb-like block polyether. *Polym. Adv. Technol.* **2018**, *29*, 3171−3180.
(57) Alvarez, F.; Flores, E. A.; Castro, L. V.; Hernández, J. G.; López, A.; Vázquez, F. Dissipative Particle Dynamics (DPD) Study of Crude Oil−Water Emulsions in the Presence of a Functionalized Copolymer. *Energy Fuels* **2010**, *25*, 562−567.
(58) Guan, D.; Feng, S.; Zhang, L.; Shi, Q.; Zhao, S.; Xu, C. Mesoscale Simulation for Heavy Petroleum System Using Structural Unit and Dissipative Particle Dynamics (SU−DPD) Frameworks. *Energy Fuels* **2019**, *33*, 1049−1060.
(59) Maiti, A.; McGrother, S. Bead-bead interaction parameters in dissipative particle dynamics: relation to bead-size, solubility parameter, and surface tension. *J. Chem. Phys.* **2004**, *120*, 1594−1601.
(60) Rezaei, H.; Amjad-Iranagh, S.; Modarress, H. Self-Accumulation of Uncharged Polyaromatic Surfactants at Crude Oil−Water Interface: A Mesoscopic DPD Study. *Energy Fuels* **2016**, *30*, 6626−6639.
(61) Li, Y.; Guo, Y.; Bao, M.; Gao, X. Investigation of interfacial and structural properties of CTAB at the oil/water interface using dissipative particle dynamics simulations. *J. Colloid Interface Sci.* **2011**, *361*, 573−580.
(62) Duan, M.; Song, X.; Zhao, S.; Fang, S.; Wang, F.; Zhong, C.; Luo, Z. Layer-by-Layer Assembled Film of Asphaltenes/Polyacrylamide and Its Stability of Water-in-Oil Emulsions: A Combined Experimental and Simulation Study. *J. Phys. Chem. C* **2017**, *121*, 4332−4342.
(63) Wang, S.; Xu, J.; Wen, H. Dissipative particle dynamics simulation on the rheological properties of heavy crude oil. *Mol. Phys.* **2015**, *113*, 3325−3335.
(64) Goodarzi, F.; Zendehboudi, S. Effects of Salt and Surfactant on Interfacial Characteristics of Water/Oil Systems: Molecular Dynamic Simulations and Dissipative Particle Dynamics. *Ind. Eng. Chem. Res.* **2019**, *58*, 8817−8834.
(65) Xu, Y.; Yu, X.; Yan, H.; Wang, Y.; Feng, J. Self-Assembly Behaviors of Heterogemini Surfactant in Aqueous Solution Investigated by Dissipative Particle Dynamics. *J. Dispersion Sci. Technol.* **2014**, *35*, 1300−1307.
(66) Rezaei, H.; Modarress, H. Dissipative Particle Dynamics Study of Interfacial Properties and the Effects of Nonionic Surfactants on Hydrocarbon/Water Microemulsions. *J. Dispersion Sci. Technol.* **2015**, *37*, 969−979.
(67) Wang, Z.; Li, Y.; Guo, Y.; Zhang, H. Investigations of Interfacial Properties of Surfactants with Different Structures at the Oil/Water Interface Using Dissipative Particle Dynamics. *J. Dispersion Sci. Technol.* **2013**, *34*, 1020−1028.
(68) Jiang, H.; Liu, X.; Liang, C.; Wang, Z.; Jia, Y. Dissipative particle dynamics to study asphaltenes and surfactants interactions at the oil-water interface. *J. Mol. Liq.* **2023**, *381*, 121802.
(69) Groot, R. D. Electrostatic Interactions in Dissipative Particle Dynamics-Simulation of Polyelectrolytes and Anionic Surfactants. *J. Chem. Phys.* **2003**, *118*, 11265−11277.
(70) Groot, R. D.; Rabone, K. Mesoscopic Simulation of Cell Membrane Damage, Morphology Change and Rupture by Nonionic Surfactants. *Biophys. J.* **2001**, *81*, 725−736.
(71) Groot, R. D.; Warren, P. B. Dissipative particle dynamics: Bridging the gap between atomistic and mesoscopic simulation. *J. Chem. Phys.* **1997**, *107*, 4423−4435.
(72) de Oliveira, F. C.; Khani, S.; Maia, J. M.; Tavares, F. W. Concentration and Solvent Effects on Structural, Dynamical, and Rheological Properties of Asphaltene Suspensions. *Energy Fuels* **2019**, *34*, 1071−1081.
(73) Cheng, Y.; Yuan, S. Emulsification of Surfactant on Oil Droplets by Molecular Dynamics Simulation. *Molecules* **2020**, *25*, 3008.
(74) Skartlien, R.; Simon, S.; Sjöblom, J. A DPD study of asphaltene aggregation: The role of inhibitor and asphaltene structure in diffusion-limited aggregation. *J. Dispersion Sci. Technol.* **2016**, *38*, 440−450.

https://doi.org/10.1021/acsomega.3c05486
ACS Omega 2023, 8, 33083−33097